Dynamic Actuation of Single-Crystal Diamond Nanobeams

Young-Ik Sohn, Michael J. Burek, and Marko Lončar*

School of Engineering and Applied Sciences, Harvard University, 29 Oxford Street, Cambridge, Massachusetts 02138, United States

E-mail: loncar@seas.harvard.edu

Abstract

We show the dielectrophoretic actuation of single-crystal diamond nanomechanical devices using gradient radio-frequency electromagnetic forces. Both cantilever and doubly clamped beams, fabricated using our angled-etching fabrication technique,[1] are demonstrated, with operation frequencies ranging from a few MHz to ∼50 MHz. Frequency tuning and parametric actuation are also studied.

Owing to its large Young's modulus, excellent thermal properties, small thermo-elastic dissipation, *single-crystal* diamond is an ideal candidate for realization of high-frequency (f) and high quality factor (Q) nanoscale mechanical resonators. These devices are of interest for realization of stable, high $f \cdot Q$ product, RF oscillators and inertial sensing applications.[2] Recently, diamond nanomechanical resonators embedded with luminescent crystalline defects (color centers), have also been explored as a promising platform for applications in quantum information

---

*To whom correspondence should be addressed

1

science and technology (QIST).[3] Of these, negatively charged nitrogen-vacancy (NV$^-$) color center is of particular interest since it can be used as a spin-qubit with optical read-out. Importantly, NV$^-$ electron spin state can have long coherence times (milliseconds)[4] even at room temperature and it can be prepared and manipulated using microwave and radio frequency (RF) fields to drive transitions between these electron and nuclear spin sublevels.[5–7] Recently, it has been proposed that strain-fields can also be used to manipulate the spin-state of NV,[8,9] which resulted in renewed interest of QIST community in single-crystal diamond micro-electromechanical systems (MEMS).[10–12] For example, coupling between an NV$^-$ center and a mechanical resonator could enable high fidelity control of NV$^-$ spin state via rapid adiabatic passage,[10] and potentially the remote coupling of NV centers via mechanics.[3] Furthermore, mechanical resonators may enable coherent coupling between dissimilar systems with degrees of freedom possessing dramatically different properties and energy scales. To realize such systems, it is essential to achieve a reliable method for controlling and reading the dynamic action of monolithic single-crystal diamond mechanical resonators. To date, several reports have demonstrated mechanical resonators fabricated in single-crystal diamond,[13–18] with recent results demonstrating the coupling of NV$^-$ centers to bulk phonon modes[10,19] and micron-scale mechanical resonators.[11,12] Of these, cantilever device using strain at its clamp induced from the driven motion[11,12]is a promising platform, due to its large applicable stress. Hundreds of MPa is achievable at the clamp of 600 nm thick, 24μm long cantilever at 25 dBm drive power of piezo transducer,[20] compared to 10 MPa at 25 dBm drive of HBAR resonator.[10] Furthermore, dynamic driving of cantilevers with resonances above 10 MHz, and in particular at frequencies larger than electron-spin resonance linewidth, is required for reaching so called resolved sideband regime.[12] In general, there is a trade-off between achievable maximum strain at unit drive power and resonance frequency. This work aims at achieving high frequency dynamic actuation of flexural mechanical mode in single-crystal diamond as well as large strain-fields at the site of NV$^-$ center.

Dielectrophoretic actuation[21] has recently been used to actuate and transduce motion of nanoelectromechanical systems (NEMS) and applied to achieve mechanical resonance tuning,[22] and

coherent control of classical mechanical resonators,[23] as well as to study cavity electromechanics,[24] and nonlinear mechanics.[25] In our approach, single-crystal diamond cantilevers (Figure 1(a)) and doubly clamped nanobeams (Figure 1(b)) are placed between metal electrodes and are driven by fringing radio-frequency (RF) field (Figure 1(c)) with frequency resonant with mechanical resonance of the devices. Our numerical modeling indicates that keeping small vertical distance from electrodes to nanobeam is of crucial importance for efficient actuation (Figure 1(d)).

In contrast to conventional electrostatic and piezo-electric actuation approaches, that may require physical contact or doping of diamond nanomechanical structure, gradient RF force does not require any modification to the mechanical resonator itself. Therefore, it preserves diamond's unique material properties (Young's modulus, low mass density, large thermal conductivity, and low thermoelastic dissipation) thus minimizing dissipations and resulting in devices with large mechanical quality factors. Of particular interest for QIST applications, dielectrophoretic actuation scheme maintains the integrity and stability of NV centers embedded within diamond nanomechanical structures, that are known to be sensitive to fabrication imperfections and surface terminations.[26] Additionally, we note that electrodes employed for actuation may also double for on-chip delivery of microwave power to NV$^-$ center. Therefore, we believe that dielectrophoretic actuation is an ideal choice for investigation of NV-mechanical coupling.

Our diamond cantilevers and doubly clamped beams are fabricated using fabrication technique–angled-etching–that we have recently developed,[1] which is shown in Figure 2(a). Briefly, angled-etching employs anisotropic oxygen plasma etching at an oblique angle to the substrate surface, yielding suspended triangular cross-section nanobeams directly from single-crystal bulk diamond substrates. Nanomechanical resonators fabricated by angled-etching are easily integrated with dielectrophoretic actuation. Parameters for nanobeam width and the distance from the bottom apex of the nanobeams to the substrate have to be carefully chosen in order to maximize the efficiency of transduction (Figure 1(c) and (d)). See *Supporting Information* for further discussion. Once free-standing diamond nanobeams were fabricated, electrodes were patterned on the diamond substrate via a standard metal lift-off process. First, the diamond substrate was spin coated with a

3

polymethylmethacrylate-copolymer (MMA/PMMA) bilayer resist, where the MMA copolymer thickness was carefully chosen to be slightly thicker than the distance between the nanobeam top surface and the substrate. Conformal resist coating was observed, without any complication due to existing device geometry. After resist coating, exposure and alignment were done via electron beam lithography. 50 nm of titanium and 200 nm of gold layer were then evaporated and followed by lift-off in remover PG to complete electrode patterning. Figure 2(b) is a top-down view of diamond nanobeam cantilever. It can be seen that good alignment can be achieved, with error on the order of tens of nanometer – this is more than adequate for efficient actuation. In fact, we note that the slight misalignment is actually beneficial since it enables the actuation of in-plane motion, as discussed below. Figure 2(c) shows an array of fabricated diamond doubly clamped nanobeam mechanical resonators that share driving electrodes. This configuration allows us to characterize in parallel large number of resonators having slightly different geometry and hence different resonance frequencies. Our nanomechanical resonators had wide range of widths (200 nm - 300 nm) and lengths (1 μm - 20 μm), corresponding to fundamental flexural resonance frequencies (from Euler-Bernoulli beam theory) ranging from a few MHz to hundreds of MHz. Due to the nature of angled-etching fabrication technique, width and thickness of nanobeam's triangular cross-section are correlated. The smallest cantilever that could be characterized (Figure 1(a)) had a width of 300 nm and the length of 4 μm, while the smallest doubly clamped nanobeam (Figure 1(b)) had a width of 200 nm and the length of 7 μm.

All experiments were performed at room temperature, inside a vacuum chamber at the pressure below 10^{-5} Torr. Figure 3(a) shows a schematic of the experimental setup, which is a slightly modified version of that used previously for characterizing the Brownian motion of single-crystal diamond nanobeams.[17] Specifically, network analyzer was used instead of spectrum analyzer in order to obtain driven response of our devices (by sweeping the driving frequency around mechanical resonance), and a bias-tee was included to combine DC bias with RF drive signal to ensure proper actuation: since actuation force is proportional to the square of applied voltage, $F \propto (V_{DC} + V_{RF} \cos \omega t)^2$.[21] DC bias is needed to provide force component at the driving frequency.

For the most of fabricated diamond nanobeams, both the fundamental out-of-plane and in-plane modes were characterized. Resonant responses of fundamental out-of-plane motion of devices shown in Figure 1(a) and (b) are plotted in Figure 3(b) and (c), respectively. Solid curves are fitted to the raw data, with both figures showing the expected resonant responses in the linear regime. The maximum resonant frequency of the out-of-plane mode that we could measure using our approach was ~40 MHz, in the case of 7 μm long doubly clamped nanobeam. The maximum resonant frequency of the in-plane mode, measured in the same devices, was ~50 MHz. To the best of our knowledge, this is the highest actuation frequency of flexural mechanical vibration achieved by dielectrophoretic actuation to date. Unfortunately, in our current experiments, we were not able to measure devices with resonances >50 MHz, due to the deteriorated signal-to-noise ratio of our measurements. Noise floor of our experiment was affected by three different instruments: shot noise from laser source, dark current and thermal noise from photodetector and thermal noise from the receiver, which can be either the network analyzer or spectrum analyzer. Depending on the settings of instruments, any of these three could be the limiting factor for the noise floor. Most of our measurements, however, were limited by the shot noise from the laser source.

In many MEMS / NEMS applications, high $f \cdot Q$ product is an important figure of merit to get a high sensitivity. State-of-the-art flexural NEMS device can reach $f \cdot Q$ product of 6.8×10^{12} Hz.[27] In our devices, maximum $f \cdot Q$ product that we measured was 2.35×10^{11} Hz in the case of 300 nm wide and 4 um long cantilever ($f = 38$ MHz). We note that all devices that we characterized have comparable mechanical Qs, regardless of their length and operating frequency. Therefore, we believe that currently Q is limited by surface losses, since all devices have comparable surface to volume ratio.[28] This fact is different from what we previously reported,[17] which indicates the clamping loss as a dominant loss mechanism. Possible explanation would be that the nanobeams in this work have larger surface to volume ratio due to its smaller widths (200 nm - 300 nm compared to ~ 1 μm in previous study), hence they have larger contribution from surface loss.

By further increasing the input RF power, and by using longer devices having smaller spring constant, the diamond nanomechanical structures could be driven deep into the nonlinear regime

(Figure 4). We note that longer devices are "softer" and therefore deflect more for the same applied voltage, thus easily entering nonlinear regime with the same driving power. Typically, nonlinearity in small scale mechanical resonators can be phenomenologically modeled using Duffing equation:

$$\left[\frac{d^2}{dt^2} + \frac{\Omega_0}{Q} \frac{d}{dt} + \Omega_0^2 \left(1 + \beta x^2(t) \right) \right] x(t) = \frac{F(t)}{m} \tag{1}$$

where $x(t), \Omega_0, Q, F(t)$ and m are the beam displacement, the resonance frequency, mechanical quality factor, external driving force and effective mass of the resonator, respectively. The cubic term $\beta x^3(t)$ in the equation, so called 'Duffing nonlinearity', determines the nonlinear behavior of the resonator: when $\beta < 0$ resonance tends to move to the lower frequency when amplitude increases, resulting in "softening", that is lowering of the spring constant; the opposite is true when $\beta > 0$ and spring "hardening" occurs. Figure 4(a) and (b) show softening of the fundamental out-of-plane and in-plane modes, respectively, for 8 μm long diamond nanobeam cantilever. On the other hand, spring hardening is observed in the case of 13 μm long doubly clamped diamond nanobeam, for both out-of-plane and in-plane modes shown in Figure 4(c) and (d), respectively.

There are many physical origins that can give rise to mechanical nonlinearities, including, but are not limited to transduction effects, actuation scheme, material properties, non-ideal boundary conditions, damping mechanics and geometric/inertial effects.[29] Based on our FEM simulations and dipole approximation for force calculation, we believe that in our case nonlinearity is due to either nonlinear actuation or geometry. Actuation nonlinearity can either cause hardening or softening depending on the beam separation from the driving electrodes (Figure 1(c)). On the other hand, geometric nonlinearity, which could be analytically calculated by considering axial inertia and nonlinear curvature, always induces hardening.[30] In the case of cantilevers, shown in Figure 4 (a) and (b), both modes show softening which can be explained by nonlinear actuation. As for doubly clamped beams, tension-induced geometric nonlinearity is dominant within device parameter space explored in this work. Therefore hardening in Figure 4 (c) and (d) can be explained from tension-induced effect. See *Supporting Information* for details.

Nonlinear behavior was further confirmed by hysteresis curves as shown in Figure 5(a) and (b), which are measured from fundamental out-of-plane and in-plane modes of 19 μm long doubly clamped diamond nanobeam, respectively. This device was particularly chosen among others as a representative examples because of its prominent nonlinearity, though, other devices gave the hysteresis curves as expected.

Our dielectrophoretic actuation scheme introduces an additional effective spring since the actuation force has dependence on position.[21] Furthermore, since the force has a quadratic dependence on applied voltage, the mechanical eigenfrequency is tunable with DC bias, and the amount of shift in frequency has quadratic dependence on voltage. Figure 6 (a) shows Brownian motion measured with a spectrum analyzer as the applied DC bias was changed from -9 V to $+9$ V. Bright spots of each data column correspond to the Brownian motion resonance location. The solid black line is a quadratic fit for applied DC bias and shows an excellent match with the theoretical prediction. In the given range of applied DC bias, the mechanical resonance could be tuned over roughly 260 full width at half maximum of the zero bias Brownian motion peak. We observe a blue shift of resonance frequency because this motion is in-plane vibration and the effective spring has always the same sign with the elastic spring. In the case of out-of-plane modes, frequency tuning can be either red or blue shifted, depending on the height of the beam from the driving electrodes.[22]

Since the resonance frequency is easily parametrically tuned much more than a linewidth, parametric excitation is also expected. Criteria for a resonator to be used for parametric actuation is given in equation (**??**).[31]

$$\left. \frac{\partial f}{\partial V} \right|_{V_{max}} \cdot V_{max} \cdot \frac{Q}{f_0} > 2 \tag{2}$$

where f, V and Q are resonance frequency, amplitude of applied RF voltage and mechanical quality factor, respectively. f_0 is a resonance frequency without RF voltage input and V_{max} represents the maximum voltage that can be applied. Since the spring constant is a function of position, it can be modeled with Mathieu's equation with a Duffing nonlinearity. Equation (**??**) may be modified to

include parametric tuning as shown below:

$$\left[\frac{d^2}{dt^2} + \frac{\Omega_0}{Q}\frac{d}{dt} + \Omega_0^2 \left(1 + \alpha + \beta x^2(t) - 2\Gamma\sin 2\Omega_0 t\right)\right] x(t) = 0 \tag{3}$$

where α is the detuning between the parametric excitation and the fundamental mode Ω_0, Γ is proportional to the parametric excitation amplitude,[32] whereas other parameters are defined the same way as in equation (??). Right hand side of the equation (??) is zero, since there was no direct driving at resonance frequency. When the resonator with eigenfrequency f_0 can be parametrically excited, its excitation frequency can be $\frac{2f_0}{n}$ for any integer n. In most of the cases, response at $n = 1$ is used since it is the strongest, although the submultiples of it has been observed in experiment.[33] Mathieu's equation with Duffing nonlinearity (??) can be analytically solved and the solution predicts its stability on a phase plane, axes of which are detuning and driving amplitude. Here, we show "instability tongue"[34] when doubly clamped diamond nanobeam is parametrically excited with $n = 1$. In Figure 6(b) the measured instability tongue is shown when nanobeam was excited around the twice of its natural frequency of 7.25 MHz. In this experiment, excitation was done by RF signal generator and the response was measured with spectrum analyzer, with the amplitude of driven motion was calculated by simple signal processing. Parametric excitation is particularly interesting for NEMS devices since it can circumvent electric cross talk, which can be detrimental for nanoscale system,[35] and can be used to realize a NEMS oscillator[31] and mechanical memory element.[32] Furthermore, parametric oscillators are of interest for mechanical quality factor enhancement,[36] parametric amplification,[37] and noise squeezing.[38]

In summary, we have realized a resonant actuator based on dielectrophoresis for single-crystal diamond nanomechanical resonators. Actuation of both cantilever and doubly clamped diamond nanobeams was achieved for both the fundamental out-of-plane and in-plane vibrations. Driving frequency range spans from a few MHz to nearly 50 MHz, though higher frequency actuation is expected to be realized by improving the signal-to-noise ratio of the optical interferometric displacement detection, or moving to other displacement read-out schemes with better sensitivity.

The dielectrophoretic actuation scheme employed is expected to maintain the mechanical quality factor of the base diamond device, and also to not compromise the optical properties of integrated diamond color centers.

Furthermore, our actuation scheme can efficiently drive the mechanical resonance well into the nonlinear regime, with reasonable RF power levels. Studying physical origins of mechanical non-linearity in NEMS devices are active field of research, with many open questions unanswered.[39–41] To the best of our knowledge, we believe that our work is the first demonstration of nonlinear mechanical response of single-crystal diamond resonator. Single-crystal diamond has a great potential as a nonlinear NEMS platform due to its ultrahigh mechanical quality factor over 300,000[18] or even a million at room temperature.[16]

Lastly, our actuation scheme is capable of strong frequency tuning simply by applying DC bias, and leads to useful parametric excitation. Parametric excitation is expected to be important in many applications including NV^- center engineering, since actuation signals can be completely filtered out from desired NV^- center manipulation/read-out signals in frequency domain. Single-crystal diamond actuation we developed here is expected to be a gateway to a more sophisticated platform for the control of NV^- center via nanoscale mechanics.

Acknowledgement

Supporting Information Available

A brief discussion of device design, nonlinear effect and $f \cdot Q$ product are given. This material is available free of charge via the Internet at http://pubs.acs.org/.

References

(1) Burek, M. J.; de Leon, N. P.; Shields, B. J.; Hausmann, B. J. M.; Chu, Y.; Quan, Q.; Zibrov, A. S.; Park, H.; Lukin, M. D.; Lončar, M. *Nano Letters* **2012**, *12*, 6084–6089.

(2) Kusterer, J.; Kohn, E. *CVD Diamond MEMS*; Wiley Online Library, 2009; pp 467–544.

(3) Rabl, P.; Kolkowitz, S. J.; Koppens, F. H. L.; Harris, J. G. E.; Zoller, P.; Lukin, M. D. *Nature Physics* **2010**, *6*, 602–608.

(4) Balasubramanian, G.; Neumann, P.; Twitchen, D.; Markham, M.; Kolesov, R.; Mizuochi, N.; Isoya, J.; Achard, J.; Beck, J.; Tissler, J.; Jacques, V.; Hemmer, P. R.; Jelezko, F.; Wrachtrup, J. *Nature Materials* **2009**, *8*, 383–387.

(5) van der Sar, T.; Wang, Z. H.; Blok, M. S.; Bernien, H.; Taminiau, T. H.; Toyli, D. M.; Lidar, D. A.; Awschalom, D. D.; Hanson, R.; Dobrovitski, V. V. *Nature* **2012**, *484*, 82–86.

(6) Jiang, L.; Hodges, J. S.; Maze, J. R.; Maurer, P.; Taylor, J. M.; Cory, D. G.; Hemmer, P. R.; Walsworth, R. L.; Yacoby, A.; Zibrov, A. S.; Lukin, M. D. *Science* **2009**, *326*, 267–272.

(7) Dutt, M. V. G.; Childress, L.; Jiang, L.; Togan, E.; Maze, J.; Jelezko, F.; Zibrov, A. S.; Hemmer, P. R.; Lukin, M. D. *Science* **2007**, *316*, 1312–1316.

(8) Bennett, S. D.; Yao, N. Y.; Otterbach, J.; Zoller, P.; Rabl, P.; Lukin, M. D. *Physical Review Letters* **2013**, *110*, 156402.

(9) Kepesidis, K. V.; Bennett, S. D.; Portolan, S.; Lukin, M. D.; Rabl, P. *Physical Review B* **2013**, *88*, 064105.

(10) MacQuarrie, E. R.; Gosavi, T. A.; Jungwirth, N. R.; Bhave, S. A.; Fuchs, G. D. *Physical Review Letters* **2013**, *111*, 227602.

(11) Ovartchaiyapong, P.; Lee, K. W.; Myers, B. A.; Jayich, A. C. B. *Nature Communications* **2014**, *5*.

(12) Teissier, J.; Barfuss, A.; Appel, P.; Neu, E.; Maletinsky, P. *Physical Review Letters* **2014**, *113*, 020503.

(13) Liao, M.; Rong, Z.; Hishita, S.; Imura, M.; Koizumi, S.; Koide, Y. *Diamond & Related Materials* **2012**, *24*, 69–73.

(14) Liao, M.; Hishita, S.; Watanabe, E.; Koizumi, S.; Koide, Y. *Advanced Materials* **2010**, *22*, 5393–5397.

(15) Zalalutdinov, M. K.; Ray, M. P.; Photiadis, D. M.; Robinson, J. T.; Baldwin, J. W.; Butler, J. E.; Feygelson, T. I.; Pate, B. B.; Houston, B. H. *Nano Letters* **2011**, *11*, 4304–4308.

(16) Tao, Y.; Boss, J. M.; Moores, B. A.; Degen, C. L. *Nature Communications* **2014**, *5*, 1–8.

(17) Burek, M. J.; Ramos, D.; Patel, P.; Frank, I. W.; Lončar, M. *Applied Physics Letters* **2013**, *103*, 131904–131904–5.

(18) Ovartchaiyapong, P.; Pascal, L. M. A.; Myers, B. A.; Lauria, P.; Bleszynski Jayich, A. C. *Applied Physics Letters* **2012**, *101*, 163505.

(19) MacQuarrie, E. R.; Gosavi, T. A.; Moehle, A. M.; Jungwirth, N. R.; Bhave, S. A.; Fuchs, G. D. *arXiv.org* **2014**,

(20) Meesala, S.; Sohn, Y.-I.; Atikian, H. A.; Burek, M. J.; Kim, S.; Choy, J.; Loncar, M. *in preparation*

(21) Unterreithmeier, Q. P.; Weig, E. M.; Kotthaus, J. P. *Nature* **2009**, *458*, 1001–1004.

(22) Rieger, J.; Faust, T.; Seitner, M. J.; Kotthaus, J. P.; Weig, E. M. *Applied Physics Letters* **2012**, *101*, 103110.

(23) Faust, T.; Rieger, J.; Seitner, M. J.; Kotthaus, J. P.; Weig, E. M. *Nature Physics* **2013**, *9*, 485–488.

(24) Faust, T.; Krenn, P.; Manus, S.; Kotthaus, J. P.; Weig, E. M. *Nature Communications* **2012**, *3*, 728–.

(25) Unterreithmeier, Q. P.; Faust, T.; Kotthaus, J. P. *Physical Review B* **2010**, *81*, 241405.

(26) Chu, Y.; de Leon, N. P.; Shields, B. J.; Hausmann, B. *Nano . . .* **2014**,

(27) Verbridge, S. S.; Craighead, H. G.; Parpia, J. M. *Applied Physics Letters* **2008**, *92*.

(28) Yang, J.; Ono, T.; Esashi, M. *Microelectromechanical Systems, Journal of* **2002**, *11*, 775–783.

(29) Villanueva, L. G.; Karabalin, R. B.; Matheny, M. H.; Chi, D.; Sader, J. E.; Roukes, M. L. *Phys. Rev. B* **2013**, *87*, 024304.

(30) Hamdan, M. N.; Shabaneh, N. H. *Journal of Sound and Vibration* **1997**, *199*, 711–736.

(31) Villanueva, L. G.; Karabalin, R. B.; Matheny, M. H.; Kenig, E.; Cross, M. C.; Roukes, M. L. *Nano Letters* **2011**, *11*, 5054–5059.

(32) Mahboob, I.; Yamaguchi, H. *Nature nanotechnology* **2008**, *3*, 275–279.

(33) Turner, K. L.; Miller, S. A.; Hartwell, P. G.; MacDonald, N. C.; Strogatz, S. H.; Adams, S. G. *Nature* **1998**, *396*, 149–152.

(34) Nayfeh, A. H.; Mook, D. T. *Nonlinear Oscillations*; John Wiley & Sons, 2008.

(35) Feng, X. L.; White, C. J.; Hajimiri, A.; Roukes, M. L. *Nature nanotechnology* **2008**, *3*, 342–346.

(36) Mahboob, I.; Yamaguchi, H. *Applied Physics Letters* **2008**, *92*, 253109.

(37) Suh, J.; LaHaye, M. D.; Echternach, P. M.; Schwab, K. C.; Roukes, M. L. *Nano Letters* **2010**, *10*, 3990–3994.

(38) Lifshitz, R.; Cross, M. *Reviews of nonlinear dynamics and complexity* **2008**, *1*, 1–48.

(39) Kacem, N.; Hentz, S.; Pinto, D.; Reig, B.; Nguyen, V. *Nanotechnology* **2009**, *20*, 275501.

(40) Kacem, N.; Arcamone, J.; Perez-Murano, F.; Hentz, S. *Control of buckling in large micromembranes using engineered support structures* **2010**, *20*, 045023.

(41) Imboden, M.; Williams, O.; Mohanty, P. *Applied Physics Letters* **2013**, *102*, 103502.
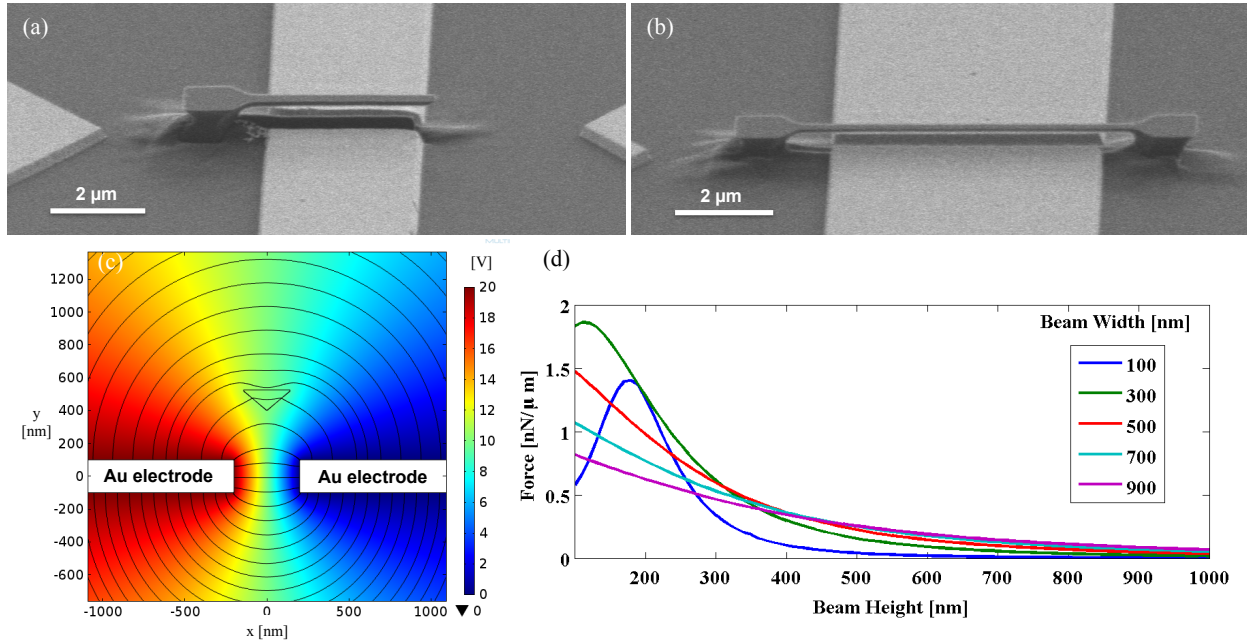
Figure 1: SEM images of (a) 4 μm cantilever and (b) 7 μm doubly clamped beam. These represent the shortest devices that could be characterized to date. (c) Finite element method (FEM) simulation is used to calculate applied force to suspended nanobeam with a given geometry and electrostatic environment. Color map stands for the voltage and the streamlines show corresponding electric field. (d) Vertical force per unit length applied to the beam from (c) is plotted as a function of beam width and height, 20 V was assumed. It can be seen that there is an optimal height that maximizes the force, since force goes to zero in the middle of two electrodes due to the symmetry, and it also goes to zero at the far distance due to the lack of electrical field gradient. It should be noted that beam thickness is proportional to beam width by the nature of angled-etching technique.
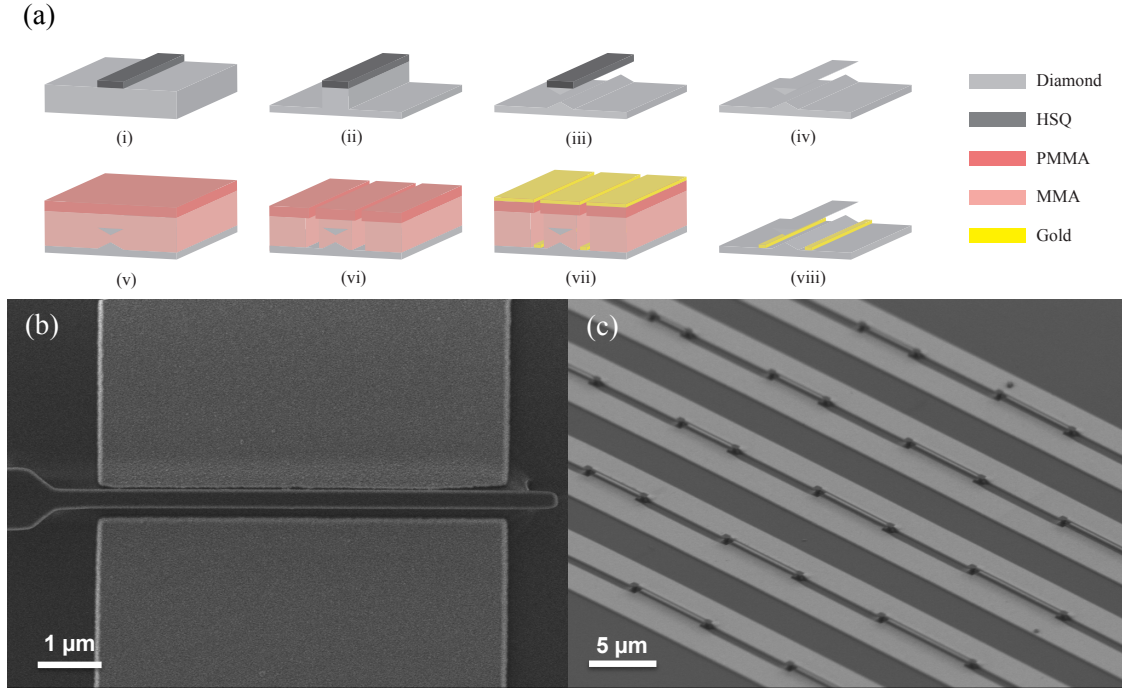
Figure 2: (a) Schematic illustration of angled-etching nanofabrication of for suspended diamond nanobeams and the following standard bi-layer MMA/PMMA process for lift-off. Each step is composed as the following: (i) Electron beam lithography mask is deposited, (ii) top-down reactive ion etching of diamond is performed, followed by the (iii) angled-etching step and (iv) mask removal. (v) New e-beam resist is deposited, and (vi) electron beam lithography followed by (vii) metal evaporation and (viii) lift-off are used to define electrodes. (b) High mag SEM image of 7 μm cantilever shows that good alignment can be achieved, on the order of tens of nanometers, which allows for efficient actuation. (c) SEM image of device array sharing electrodes.
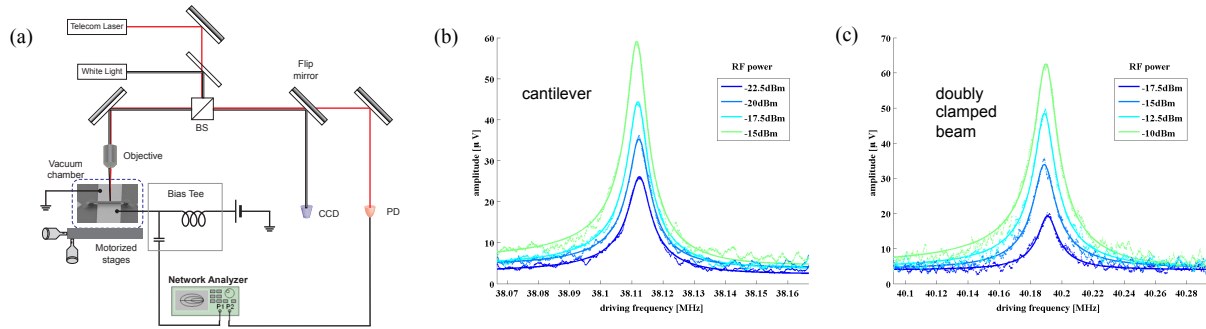

Figure 3: (a) Optical characterization setup. Fundamental out-of-plane resonant response of devices shown in Figure 1(a) and (b) are given in (b) and (c), respectively.
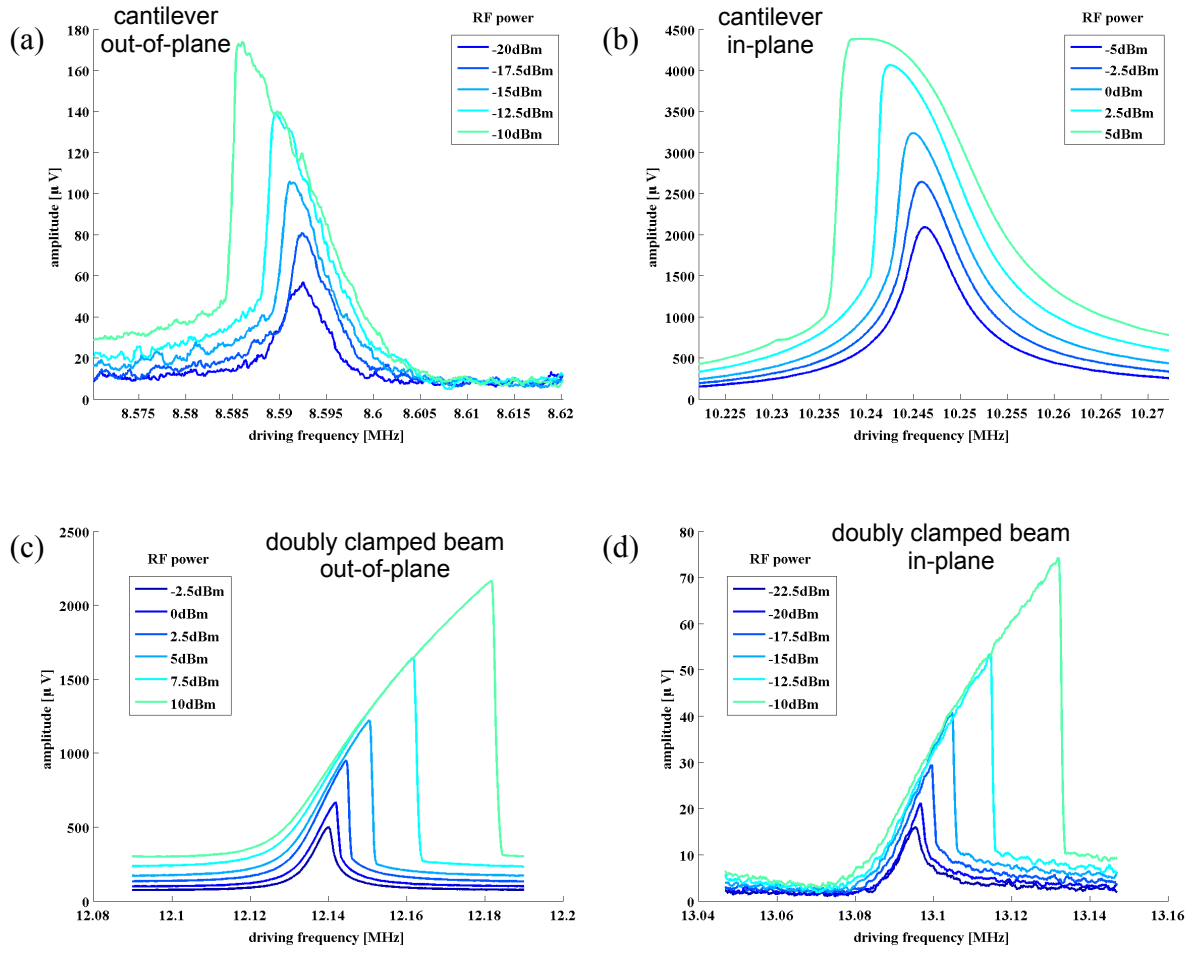
Figure 4: When nanobeams are driven hard enough, they start to show nonlinear behavior. Non-linear response of 8 μm long cantilever for its (a) out-of-plane and (b) in-plane modes. Softening of spring was observed for both types of modes. On the other hand, spring hardening was observed in the case of strongly driven 13 μm long doubly clamped diamond nanobeam both for its (c) out-of-plane and (d) in-plane modes.
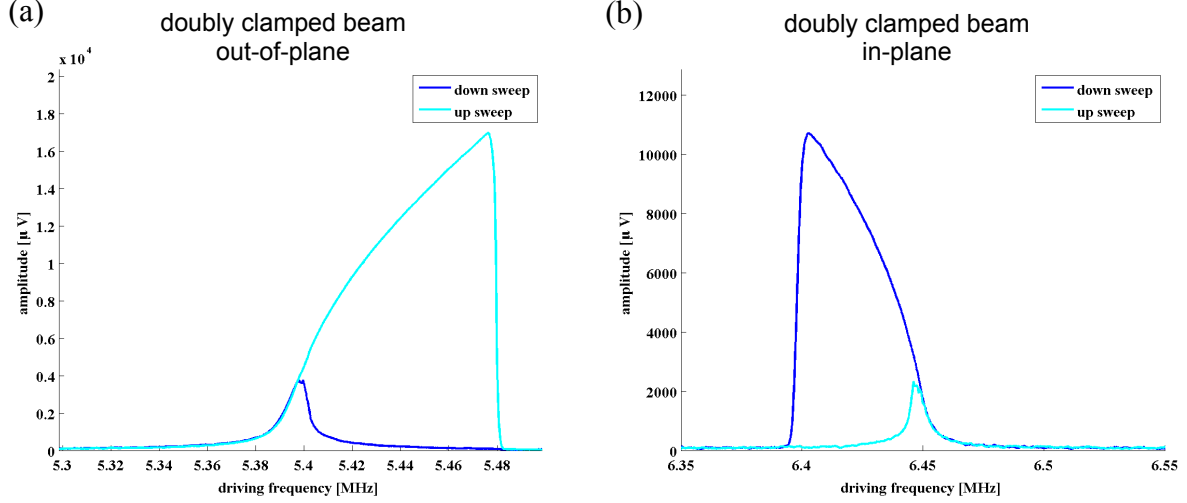
Figure 5: Hysteresis curve of (a) hardening and (b) softening mechanical nonlinearity measured from 19 μm long doubly clamped diamond nanobeam when frequency was swept up and down. (a) and (b) are the fundamental out-of-plane and in-plane modes, respectively.
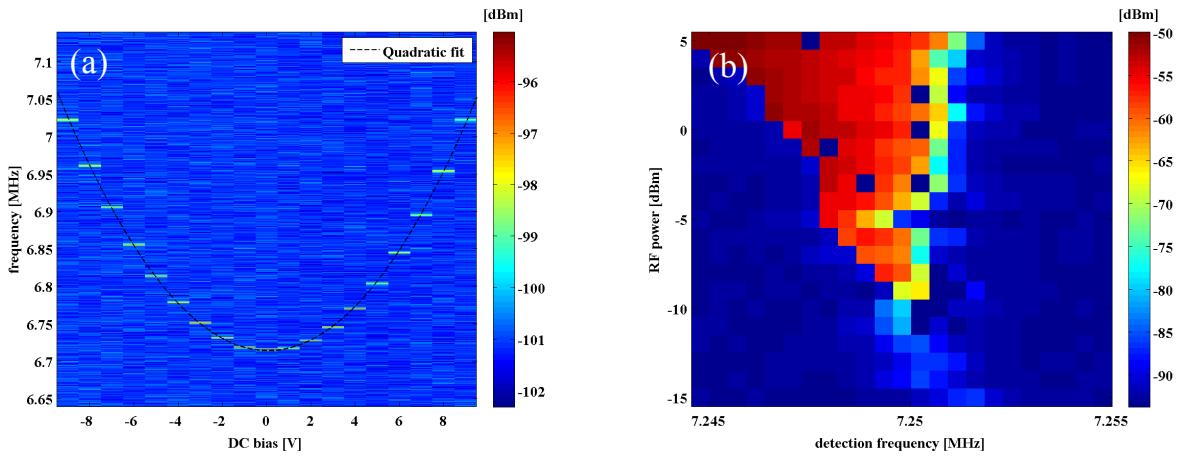

Figure 6: (a) Tuning of mechanical resonance using DC bias. With applying $\pm$9V, frequency tuning range that can be achieved is approximately 260 linewidths. Quadratic nature of tuning can be used to control the onset of parametric instability for RF power. (b) Typical tongue shape of parametric instability was observed. Low response spots inside the instability region are attributed to data acquisition software problems.

14

<div align="center">

Supporting Information

Dynamic Actuation of Single-Crystal Diamond Nanobeams

</div>

<div align="center">

Young-Ik Sohn, Michael J. Burek, and Marko Lončar[*]

School of Engineering and Applied Sciences, Harvard University, 29 Oxford Street, Cambridge,

Massachusetts 02138, United States

</div>

S1. Parameters for efficient actuation.

The amount of achievable strain at the clamp of cantilever is analyzed, in order to show how transduction efficiency and coupling strength scales with shrinking device dimension. Within our choice of angled-etching fabrication technique, when θ is given as a half of bottom apex of triangular cross section, width w and thickness t of nanobeam is related as $t = \frac{w}{2} \cot \theta$.[1] For a fixed fundamental resonance frequency $f_0 = \frac{\omega_0}{2\pi} \propto \frac{w}{L^2}$, maximum strain ϵ at clamp scales as $\epsilon \propto f_0 x_0$,[2] where L is the length of cantilever and x_0 is the displacement at the tip. For a zero

---

[*] To whom correspondence should be addressed

point motion $x_{\text{ZPM}} = \sqrt{\dfrac{\hbar}{2m_{\text{eff}}\omega_0}}$, induced strain scales as $\epsilon_{\text{ZPM}} \propto f_0 x_{\text{ZPM}} \propto g_0 \propto \sqrt{1/wL^3}$, where

g_0 is the single-phonon coupling strength. For a fixed voltage V, applied force to the cantilever

should be taken into account. After simple calculation, it can be shown that $\epsilon_V \propto \dfrac{P_0(V)}{w^2}$, where

$P_0(V)$ is the force per length as a function of applied voltage V. $P_0(V)$ is a function of the

geometry and is proportional to V^2. By assuming optimal configuration such that maximizes the

force, ϵ_V for 50-300 nm wide cantilevers is calculated from FEM (Finite Element Method) as in

Figure S1. In conclusion, smaller geometry works favorably both for the single-phonon

coupling strength and the coupling strength at a fixed voltage. In practice, fabrication and NV

stability will set the limit of achievable device size and hence the coupling rate. In this work,

200-300 nm is chosen as nanobeam width for the ease of fabrication as well as the ease of read-
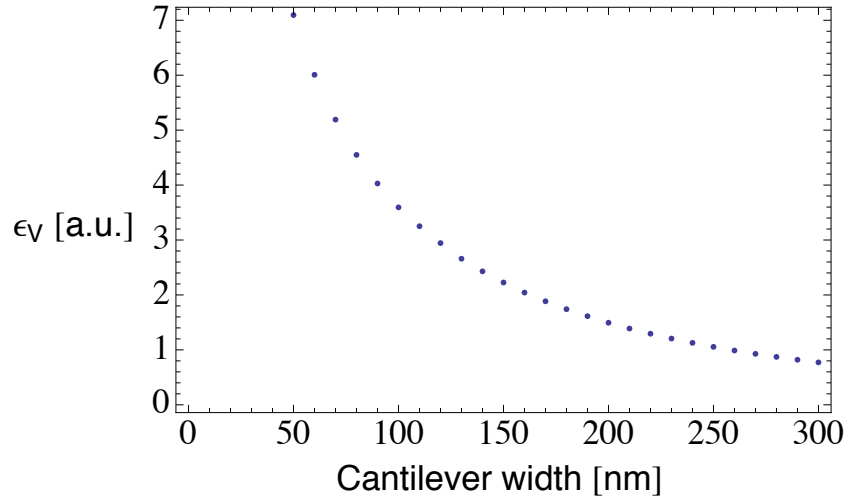
out.

Figure S1. Strain at the clamp of cantilever, for the target fundamental resonance frequency,

increases as the device width (and height) decreases.

S2. Nonlinearity from dielectrophoretic force

Due to the configuration of dielectrophortic actuation, applied force has nonlinear components. Since nanobeams have other known origins of nonlinear response,[3] it is worthwhile to do order of magnitude analysis. Taking both geometric and actuation nonlinearities into account, Duffing equation can be expressed as in equation (S1).

$$\left[\frac{d^2}{dt^2} + \frac{\Omega_0}{Q}\frac{d}{dt} + \Omega_0^2\left(1 + (\beta_{geom} + \beta_{actu})x^2(t)\right)\right]x(t) = \frac{F(t)}{m} \tag{S1}$$

where β_{geom} and β_{actu} are Duffing parameters originate from geometrical and actuation nonlinearities each.

Calculating β_{actu} from FEM is tedious and almost impossible in some cases. However, in our system, by approximating nanobeam cross-section as a dipole and electrodes as point charges,[4] it is possible to obtain simple analytic expression for actuation force. Goodness of dipole approximation can be checked in **Figure S2**(a), where FEM simulation is compared to it. Taking power series of actuation force calculated by dipole approximation and considering both parametric and cubic terms,[5] β_{actu} can be calculated for 8 μm long cantilever as in **Figure S2**(b). Note that depending on the height of nanobeam, β_{actu} can be either positive or negative. In the case of the cantilever, Duffing parameter can be calculated analytically by taking into account axial inertia and nonlinear curvature as in equation (S2).[6]

$$\beta_{geom} = \frac{EI}{L^5}\int_0^1 \phi(\xi)'^2\phi(\xi)''^2 d\xi \tag{S2}$$

where L is the length of the cantilever, E is Young's modulus, I is the second moment of area, $\phi(\xi)$ is normalized mode shape, ξ is normalized distance along the beam axis and primes denote spatial derivatives. **Figure S2**(c) shows how Duffing parameters scale with the length of cantilever. Since $\beta_{geom} > 0$, softening behavior of cantilevers in Figure 4(a) can be explained from nonlinearity of actuation force. In case of the doubly clamped beam, tension-induced

nonlinearity[7] $\beta_{geom} = \frac{EA}{2L^3}\left(\int_0^1 \phi(\xi)'^2 d\xi\right)^2$, where A is the cross sectional area, is the most

significant factor within the parameter space used in our experiments. Therefore, as it can be

seen in **Figure S2**(d), this tension-induced nonlinearity results in hardening behavior observed in
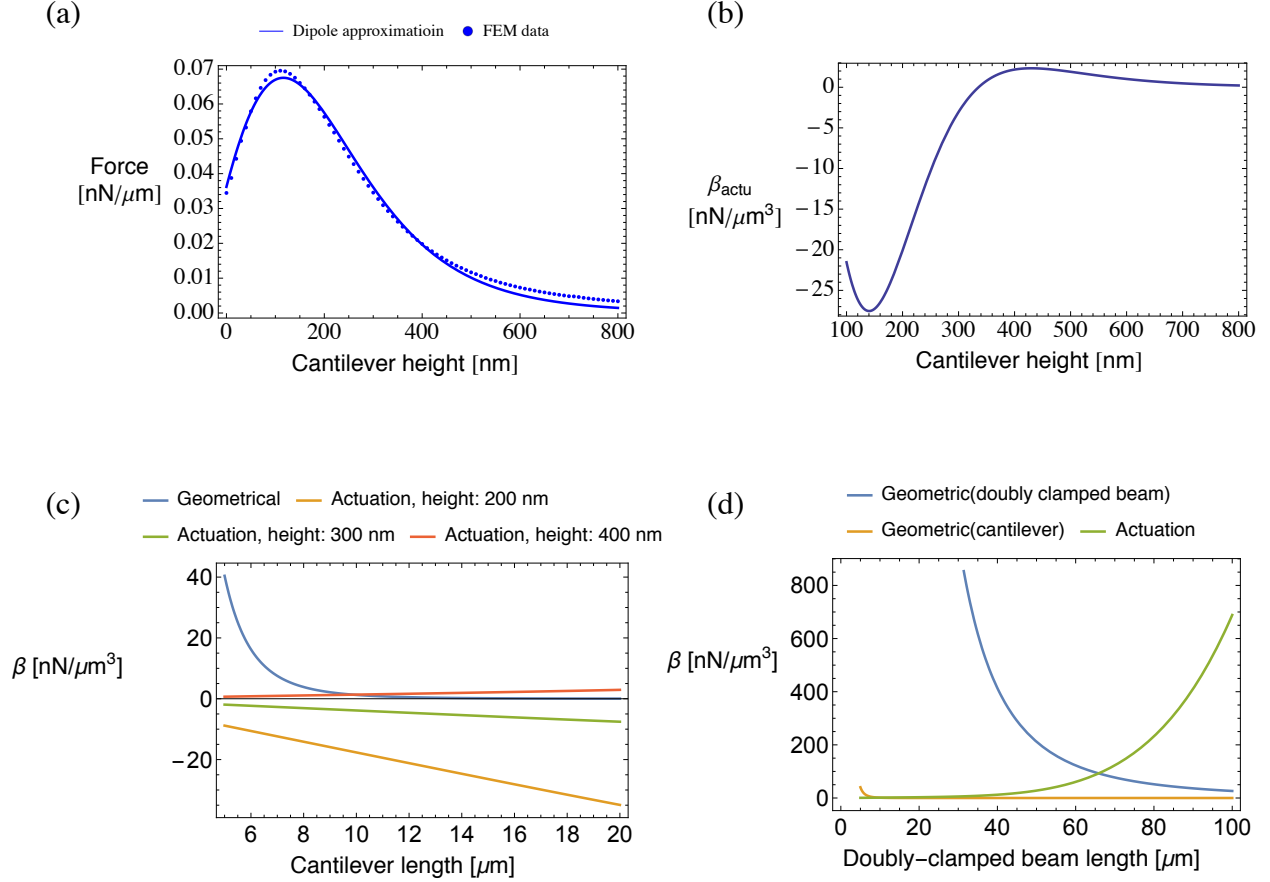
Figure 4(c).

Figure S2. (a) Comparison of applied force per unit length calculated by FEM and dipole

approximation. 300 nm wide cantilever, electrode gap of 400 nm, and applied voltage of 5 V

were used for FEM simulation. (b) Duffing parameter from nonlinear actuation force, for 8 μm

long cantilever. (c) Comparison of Duffing parameters for cantilever as a function of the length.

(d) Comparison of Duffing parameters for doubly clamped beam as a function of the length.

Beam height of 400 nm was assumed for the calculation of nonlinear actuation.

S3. $f \cdot Q$ **product of diamond nanobeams**

$f \cdot Q$ product is an important figure of merit for many high precision sensor applications.[8] Measured $f \cdot Q$ product of fabricated devices are given in **Figure S3**. From this figure, it can be seen that our devices are most likely limited by surface loss, which is supposed to give linear dependence of $f \cdot Q$ product on frequency when surface-to-volume ratio is fixed.[9]
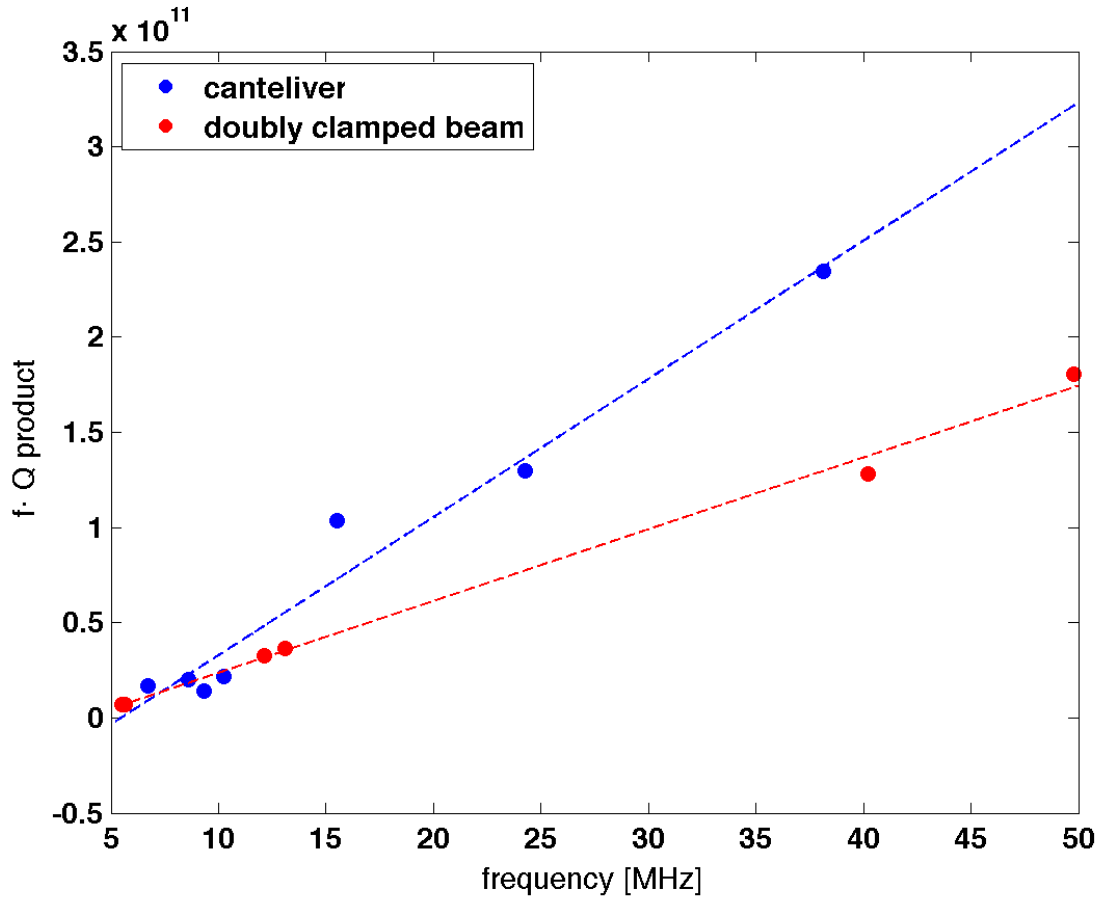

Figure S3. $f \cdot Q$ product of diamond nanobeams with linear fit. Linear relationship suggests that surface loss is likely the limiting factor of mechanical energy loss.

References:

1.	Burek, M. J.; Ramos, D.; Patel, P.; Frank, I. W.; Loncar, M. *Applied Physics Letters* **2013,** 103, (13), 131904-131904-5.
2.	Ovartchaiyapong, P.; Pascal, L. M. A.; Myers, B. A.; Lauria, P.; Bleszynski Jayich, A. C. *Applied Physics Letters* **2012,** 101, (16), 163505.
3.	Villanueva, L. G.; Karabalin, R. B.; Matheny, M. H.; Chi, D.; Sader, J. E.; Roukes, M. L. *Physical Review B* **2013,** 87, (2), 024304.
4.	Unterreithmeier, Q. P.; Weig, E. M.; Kotthaus, J. P. *Nature* **2009,** 458, (7241), 1001-1004.
5.	Kozinsky, I.; Postma, H. W. C.; Bargatin, I.; Roukes, M. L. *Applied Physics Letters* **2006,** 88, (25), 253101.
6.	Hamdan, M. N.; Shabaneh, N. H. *Journal of Sound and Vibration* **1997,** 199, (5), 711-736.
7.	Schuster, H. G., *Reviews of nonlinear dynamics and complexity*. Wiley Online Library: 2008.
8.	Verbridge, S. S.; Craighead, H. G.; Parpia, J. M. *Applied Physics Letters* **2008,** 92, (1).
9.	Yang, J.; Ono, T.; Esashi, M. *Microelectromechanical Systems, Journal of* **2002,** 11, (6), 775-783.